Structural length-scale sensitivities of reflectance measurements in continuous random media under the Born approximation

Andrew J. Radosevich,* Ji Yi, Jeremy D. Rogers, and Vadim Backman

Biomedical Engineering, Northwestern University, Evanston, Illinois 60208, USA

**Corresponding author: arad@u.northwestern.edu*

Received October 11, 2012; accepted November 14, 2012;
posted November 26, 2012 (Doc. ID 177894); published December 13, 2012

Which range of structures contributes to light scattering in a continuous random media, such as biological tissue? In this Letter, we present a model to study the structural length-scale sensitivity of scattering in continuous random media under the Born approximation. The scattering coefficient μ_s, backscattering coefficient μ_b, anisotropy factor g, and reduced scattering coefficient μ_s^* as well as the shape of the spatial reflectance profile are calculated under this model. For media with a biologically relevant Henyey–Greenstein phase function with $g \sim 0.93$ at wavelength $\lambda = 633$ nm, we report that μ_s^* is sensitive to structural length-scales from 46.9 nm to 2.07 μm (i.e., $\lambda/13$ to 3λ), μ_b is sensitive from 26.7 to 320 nm (i.e., $\lambda/24$ to $\lambda/2$), and the spatial reflectance profile is sensitive from 30.8 nm to 2.71 μm (i.e., $\lambda/21$ to 4λ).

OCIS codes: 290.5825, 290.7050, 170.3660.

Elastic light scattering provides a valuable tool to *detect* and *quantify* subdiffractional structures even if they cannot be *resolved* by a conventional imaging system. However, the limits of the sensitivity of light scattering to different structural length-scales in a continuous random media (e.g., biological tissue) have not yet been fully studied. In this Letter, we present the methodologies used to study the length-scale sensitivities of the scattering parameters μ_s, μ_b, g, and μ_s^* as well as the diffuse reflectance profile in continuous random media.

Consider a statistically homogeneous random medium composed of a continuous distribution of fluctuating refractive index, $n(\vec{r})$. We define the excess refractive index which contributes to scattering as $n_\Delta(\vec{r}) = n(\vec{r})/n_o - 1$, where n_o is the mean refractive index. Since $n_\Delta(\vec{r})$ is a random process, it is mathematically useful to describe the distribution of refractive index through its statistical autocorrelation function $B_n(r_d) = \int n_\Delta(\vec{r}) n_\Delta(\vec{r} - r_d) \mathrm{d}\vec{r}$.

One versatile model for $B_n(r_d)$ employs the Whittle–Matérn family of correlation functions [1,2]:

$$B_n(r_d) = A_n \cdot \left(\frac{r_d}{l_c}\right)^{\frac{D-3}{2}} \cdot K_{\frac{D-3}{2}}\left(\frac{r_d}{l_c}\right), \tag{1}$$

where $K_\nu(\cdot)$ is the modified Bessel function of the second kind with order ν, l_c is the characteristic length of heterogeneity, A_n is the fluctuation strength, and D determines the shape of the distribution (e.g., Gaussian as $D \to \infty$, decaying exponential for $D = 4$, and power law for $D < 3$). Importantly, when $D = 3$ this model predicts a scattering phase function that is identical to the commonly used Henyey–Greenstein model.

All light scattering characteristics can be expressed through the power spectral density Φ_s. Under the Born approximation, Φ_s is the Fourier transform of B_n [2,3]:

$$\Phi_s(k_s) = \frac{A_n l_c^3 \Gamma\left(\frac{D}{2}\right)}{\pi^{3/2} 2^{(5-D)/2}} \cdot (1 + k_s^2 l_c^2)^{-D/2}, \tag{2}$$

where $k_s = 2k \sin(\theta/2)$ and k is the wavenumber.

In order to study the sensitivity of scattering to *short* length-scales (lower length-scale analysis), we perturb $n_\Delta(\vec{r})$ by convolving with a three-dimensional Gaussian:

$$G(\vec{r}) = \left(\frac{16\pi \ln(2)}{W^2}\right)^{3/2} \cdot \exp\left(\frac{-4\ln(2)}{W^2}\vec{r}^2\right), \tag{3}$$

where W is the FWHM. Conceptually, $G(\vec{r})$ represents a process that modifies the original medium by removing "particles" smaller than W. Using the convolution theorem, this modified medium can be expressed as $n_\Delta^l(\vec{r}) = \mathcal{F}^{-1}[\mathcal{F}[n_\Delta(\vec{r})] \cdot \mathcal{F}[G(\vec{r})]]$, where $\mathcal{F}$ indicates the Fourier transform operation and the superscript l indicates that lower frequencies are retained.

The autocorrelation of $n_\Delta^l(\vec{r})$ can then be found as

$$\begin{aligned} B_n^l(r_d) &= \mathcal{F}^{-1}[|\mathcal{F}[n_\Delta(\vec{r})]|^2 \cdot |\mathcal{F}[G(\vec{r})]|^2] \\ &= 4\pi \int_0^\infty \Phi_s^l(k_s) \frac{k_s \sin(k_s r)}{r} \mathrm{d}k_s, \end{aligned} \tag{4}$$

where $\Phi_s^l(k_s)$ is the power spectral density for $n_\Delta^l(\vec{r})$ and can be computed as

$$\Phi_s^l(k_s) = \frac{A_n l_c^3 \Gamma\left(\frac{D}{2}\right)}{\pi^{3/2} 2^{(5-D)/2}} \cdot \frac{\exp\left(\frac{-k_s^2 W_l^2}{8\ln(2)}\right)}{(1 + k_s^2 l_c^2)^{D/2}}. \tag{5}$$

We note that Eq. (4) has no closed form solution, but can be evaluated numerically.

Figure 1 demonstrates the functions described by Eqs. (4) and (5) for varying values of W_l using a $B_n^l(r_d)$ with $D = 3$, $l_c = 1$ μm, and wavelength $\lambda = 633$ nm. This corresponds to a biologically relevant Henyey–Greenstein function with anisotropy factor $g \sim 0.93$. For increasing W_l, $B_n^l(r_d)$ shows a decreasing value at short length-scales [Fig. 1(a)]. The point at which $B_n^l(r_d)$ deviates from the original $B_n(r_d)$ corresponds roughly to the value of W_l. The lower value of $B_n^l(r_d)$ at short length-scales corresponds to decreased intensity

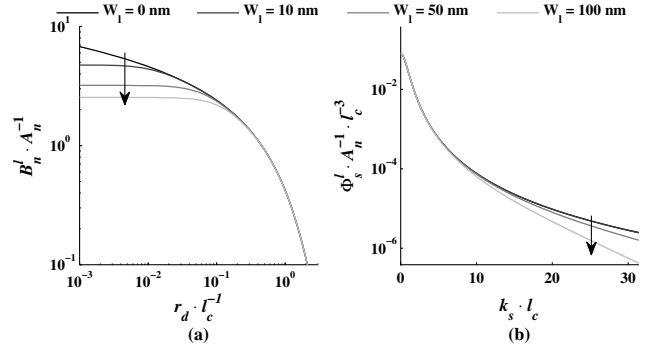

Fig. 1. Lower length-scale analysis for $W_l = 0$, 10, 50, and 100 nm with $D = 3$, $l_c = 1$ μm, and $\lambda = 633$ nm. The normalized (a) $B_n^l(r_d)$ and (b) $\Phi_s^l(k_s)$. In each panel the arrow indicates increasing W_l.

of $\Phi_s^l(k_s)$ at higher spatial frequencies after Fourier transformation [Fig. 1(b)]. To study the sensitivity of scattering to *large* length-scales (upper length-scale analysis), we employ the same model as above but filter larger particles by evaluating $n_\Delta^h(\vec{r}) = \mathcal{F}^{-1}[\mathcal{F}[n_\Delta(\vec{r})] \cdot (1 - \mathcal{F}[G(\vec{r})])]$, where the superscript h indicates that higher frequencies are retained. The autocorrelation of $n_\Delta^h(\vec{r})$ can then be found as

$$B_n^h(r_d) = \mathcal{F}^{-1}[|\mathcal{F}[n_\Delta(\vec{r})]|^2 \cdot |1 - \mathcal{F}[G(\vec{r})]|^2] = 4\pi \int_0^\infty \Phi_s^h(k_s) \frac{k_s \sin(k_s r)}{r} \mathrm{d}k_s, \quad (6)$$

where

$$\Phi_s^h(k_s) = \frac{A_n l_c^3 \Gamma\left(\frac{D}{2}\right)}{\pi^{3/2} 2^{(5-D)/2}} \cdot \frac{\left(1 - \exp\left(\frac{-k_s^2 W_h^2}{16 \ln(2)}\right)\right)^2}{(1 + k_s^2 l_c^2)^{D/2}}. \quad (7)$$

Figure 2 shows the functions described by Eqs. (6) and (7). For decreasing W_h, $B_n^h(r_d)$ exhibits a decrease at larger length-scales [Fig. 2(a)]. These alterations lead to a decreased intensity of $\Phi_s^h(k_s)$ at lower spatial frequencies [Fig. 2(b)].

As a way to visualize the continuous media represented by the above equations, Fig. 3 provides example

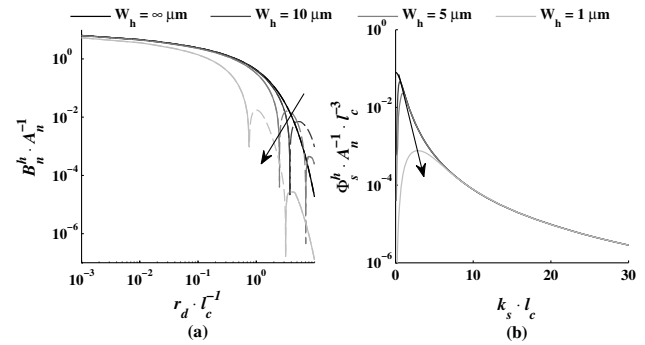

Fig. 2. Upper length-scale analysis for $W_h = \infty$, 10, 5, and 1 μm with $D = 3$, $l_c = 1$ μm, and $\lambda = 633$ nm. (a) $B_n^h(r_d)$ where the dashed curves indicate locations in which the curve is negative. (b) $\Phi_s^h(k_s)$. In each panel the arrow indicates decreasing W_h.

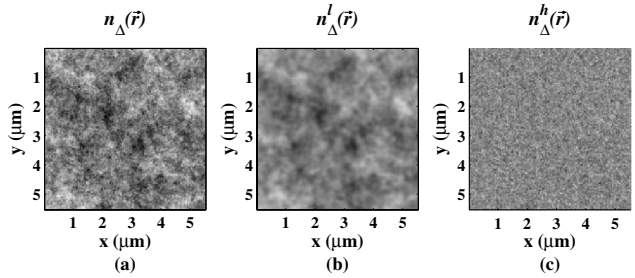

Fig. 3. Example media with $D = 3$ and $l_c = 1$ μm. (a) $n_\Delta(\vec{r})$, (b) $n_\Delta^l(\vec{r})$, and (c) $n_\Delta^h(\vec{r})$ for $W_l = W_h = 100$ nm.

cross-sectional slices through $n_\Delta(\vec{r})$, $n_\Delta^l(\vec{r})$, and $n_\Delta^h(\vec{r})$ for $D = 3$, $l_c = 1$ μm, and $W_l = W_h = 100$ nm.

Implementing the above methods, we now define a number of measurable scattering quantities. First, the differential scattering cross section per unit volume for unpolarized light $\sigma(\theta)$, can be found by incorporating the dipole scattering pattern into $\Phi_s(k_s)$:

$$\sigma(\theta) = 2\pi k^4 (1 + \cos^2\theta) \Phi_s(k_s). \quad (8)$$

The shape of $\sigma(\theta)$ can be parameterized by the scattering coefficient μ_s, the backscattering coefficient μ_b, and g [4]:

$$\mu_s = 2\pi \int_{-1}^{1} \sigma(\cos\theta) d\cos\theta, \quad (9)$$

$$\mu_b = 4\pi \cdot \sigma(\theta = \pi), \quad (10)$$

$$g = \frac{2\pi}{\mu_s} \int_{-1}^{1} \cos\theta \cdot \sigma(\cos\theta) d\cos\theta. \quad (11)$$

Conceptually, μ_s is the total scattered power per unit volume, μ_b represents the power scattered in the *backward* direction per unit volume, and g describes how *forward* directed the scattering is. Finally, the effective transport in a multiple scattering medium is expressed by the reduced scattering coefficient $\mu_s^* = \mu_s \cdot (1 - g)$.

Figure 4(a) shows percent changes in the above scattering parameters under the lower length-scale analysis for a $B_n^l(r_d)$ with $D = 3$, $l_c = 1$ μm, and $\lambda = 633$ nm. With

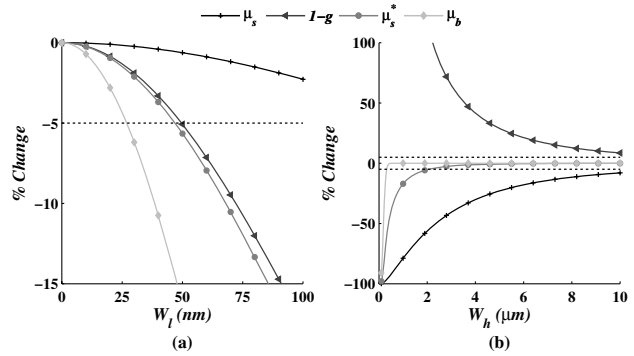

Fig. 4. Percent change in scattering parameters with varying values of W_l and W_h for $D = 3$, $l_c = 1$ μm, and $\lambda = 633$ nm. (a) Lower and (b) upper length-scale percent changes. The dotted line indicates the ±5% threshold.

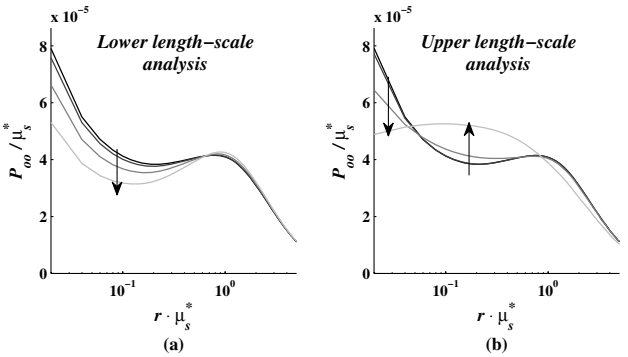

Fig. 5. Monte Carlo simulations of P_{oo} with $D = 3$, $l_c = 1$ μm, and $\lambda = 633$ nm. (a) Lower length-scale analysis for $W_l = 0$, 30, 60, and 90 nm. Arrow indicates increasing W_l. (b) Upper length-scale analysis for $W_h = \infty$, 10, 2, 0.5 μm. Arrows indicate decreasing W_h.

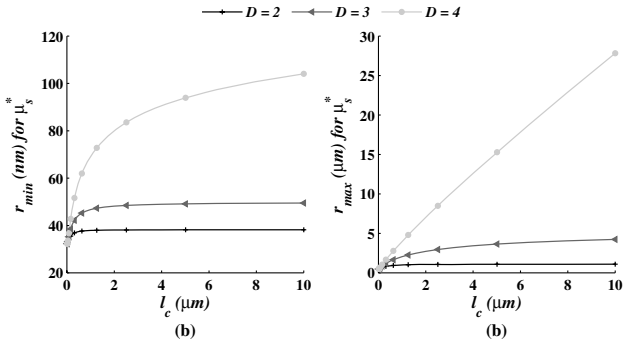

Fig. 6. (a) $r_{\min}$ and (b) $r_{\max}$ for μ_s^* with different shapes of $B_n(r_d)$ and $\lambda = 633$ nm.

increasing W_l, each parameter decreases from its original value. For μ_s, the decrease occurs because scattering material is removed from the medium. For $1 - g$ and μ_b, the decrease occurs as a result of reduced backscattering [see Fig. 1(b)]. For μ_s^*, the decrease is a combination of the previous two effects.

To provide specific length-scale sensitivity quantification, we focus on the parameters most relevant to reflectance measurements: μ_s^* for samples within the multiple scattering regime and μ_b for samples within the single scattering regime. Defining a 5% threshold (a common significance level in statistics) the minimum length-scale sensitivity ($r_{\min}$) of μ_s^* and μ_b equals 46.9 nm ($\sim\lambda/13$) and 26.7 nm ($\sim\lambda/24$), respectively. Thus, measurements of μ_s^* and μ_b provide sensitivity to structures much smaller than the diffraction limit. Interestingly, $r_{\min}$ is smaller for μ_b than μ_s^*. This can be understood by noting that k_s is maximized in the backscattering direction (i.e., $\theta = \pi$) and so provides the most sensitivity to alterations of $B_n(r_d)$ at small length-scales (see Fig. 1).

Figure 4(b) shows percent changes in the scattering parameters under the upper length-scale analysis. With decreasing W_h, μ_s decreases because scattering material is removed from the medium. For $1 - g$, an increase occurs due to a reduction in the forward scattering component. Combining these two opposing effects, the maximum length-scale sensitivity ($r_{\max}$) for μ_s^* equals 2.07 μm ($\sim 3\lambda$). For μ_b, a very small value of W_h is needed in order to alter backscattering. As a result, $r_{\max}$ for μ_b is only 320 nm ($\sim\lambda/2$).

In order to study the length-scale sensitivity of the spatial reflectance profile we performed electric field Monte Carlo simulations of continuous random medium as described in [5]. Here, we display the distribution measured with unpolarized illumination and collection, $P_{oo}(r)$. $P_{oo}(r)$ is the distribution of light that exits a semi-infinite medium antiparallel to the incident beam and within an annulus of radius r from the entrance point. It is normalized such that $\int_0^\infty P_{oo}(r)\mathrm{d}r = 1$.

Figure 5(a) shows P_{oo} under the lower length-scale analysis for a $B_n(r_d)$ with $D = 3$, $l_c = 1$ μm, and $\lambda = 633$ nm. With increasing W_l, the value of P_{oo} is decreased within the subdiffusion regime (i.e., $r \cdot \mu_s^* < 1$). This decrease can be attributed in part to the decreased intensity of the phase function in the backscattering direction [see Fig. 1(b)]. For $r \cdot \mu_s^* > 1$, a range that is essentially insensitive to the shape of the phase function, P_{oo} remains largely unchanged. Figure 5(b) shows similar results for the upper length-scale analysis. In order to perform a sensitivity analysis, we calculate the maximum percent error at any position on P_{oo} relative to the original case. Applying a 5% threshold once again, we find that $r_{\min} = 30.8$ nm ($\sim\lambda/21$) and $r_{\max} = 2.71$ μm ($\sim 4\lambda$).

Finally, we note that the exact values of $r_{\min}$ and $r_{\max}$ depend on the shape of $B_n(r_d)$. The values given above provide an estimate assuming a correlation function shape that is widely used and accepted for modeling of biological tissue (Henyey–Greenstein). Figure 6 illustrates the dependence of $r_{\min}$ and $r_{\max}$ on the shape of $B_n(r_d)$, assuming the Whittle–Matérn model and using μ_s^* as an example. As either D or l_c increases, $B_n(r_d)$ shifts relatively more weight to larger length-scales and away from smaller length-scales. As a result, both $r_{\min}$ and $r_{\max}$ increase monotonically with D and l_c.

This study was supported by National Institutes of Health grants RO1CA128641 and R01EB003682. A.J. Radosevich is supported by a National Science Foundation Graduate Research Fellowship under Grant DGE-0824162.

References

1. P. Guttorp and T. Gneiting, "On the Whittle–Matérn correlation family," National Research Center for Statistics and the Environment, Technical Report Series (2005).
2. J. D. Rogers, İ. R. Çapoğlu, and V. Backman, Opt. Lett. **34**, 1891 (2009).
3. A. Ishimaru, *Wave Propagation and Scattering in Random Media* (IEEE, 1997).
4. C. F. Bohren and D. R. Huffman, *Absorption and Scattering of Light by Small Particles* (Wiley, 1983).
5. A. J. Radosevich, J. D. Rogers, İ. R. Çapoğlu, N. N. Mutyal, P. Pradhan, and V. Backman, J. Biomed. Opt. **17**, 115001 (2012).